Determination of the Ge-nanocrystal/SiO_2 matrix interface trap density from the small signal response of charge stored in the nanocrystals

R. Peibst,[1,*] J. S. de Sousa,[2] and K. R. Hofmann[1]
[1]*Institute of Electronic Materials and Devices, Leibniz Universität Hannover, 30167 Hannover, Germany*
[2]*Departamento de Física, Universidade Ferderal do Ceará, 60455-900 Fortaleza, Brazil*
(Received 28 June 2010; published 9 November 2010)

We investigate the linear response of charge stored in Ge nanocrystals (NCs) embedded in SiO_2 to an alternating electric field in order to study the electronic properties of the Ge-NC/SiO_2 interface. Experimentally, the modulation of the cluster charge is sensed by the transient drain current of field-effect transistors in whose gate oxide the nanocrystals are embedded. For interpretation of the experimental results, we present a small-signal model obtained from a first-order expansion of the general quantum-mechanical description of the system. The contribution of trap states to the alternation of the cluster charge is distinguished from that of quantized states in the NC conduction band by calculating the latter one by density functional theory and subtracting it from the experimental values. A high Ge-NC/SiO_2 interface density of 2.8×10^{13} cm^{-2} eV^{-1} is obtained. These traps cannot be passivated efficiently by a hydrogen anneal at 450 °C and mediate efficient nonradiative recombination processes.

DOI: 10.1103/PhysRevB.82.195415 PACS number(s): 62.23.Pq, 68.35.Dv, 71.15.Mb, 78.67.Bf

I. INTRODUCTION

In the last decade, germanium nanocrystals (NCs) have been studied intensively due to their potential applications for electrical nonvolatile memories,[1–3] in optoelectronics[4,5] and in photovoltaics.[6,7] For these purposes, the Ge NCs are usually embedded in an insulating matrix. The matrix material most intensively studied so far is SiO_2 while alternative matrix materials such as GeO_2,[8] AlHfO,[9] and polymers[7] have been investigated as well.

From a theoretical point of view idealizing the Ge-NC:SiO_2 system, i.e., considering the charge carriers to be exclusively stored in quantized states of the conduction and valence band of the nanocrystal, the expected electronic and optoelectronic properties of Ge NCs are very promising. Based on tight-binding calculations, Niquet *et al.*[10] showed that the band gap of the Ge-NC can be engineered over a wide range, implying optical band-to-band transitions adjustable from the infrared to the visible regime. The predicted shift of the valence-band edge was verified experimentally by ultraviolet photoemission spectroscopy.[11] Furthermore, Takeoka *et al.*[12] reported a strong increase in the photoluminescence efficiency with decreasing NC size.

However, very little is known about the electronic properties of the interface between the Ge NCs and the SiO_2 matrix. For Si nanocrystals, recent atomistic theoretical investigations show that the Si-NC/SiO_2 interface strongly affects the electronic structure of the Si NC, implying a smaller band gap than a free-standing, hydrogen-passivated Si NC would exhibit.[13,14] Furthermore, molecular-dynamics simulations[15,16] and Monte Carlo simulations[17] show that the interface region contains strain-induced lattice distortions in the outer regions of the Si NC and a surrounding thin suboxide layer containing a considerable amount of undercoordinated defects. This interface region can be expected to exhibit a significant amount of spatially localized electronic states with energy levels within the band gap of the NC. These interface states may capture electrons and holes from the NC and therefore act as nonradiative Shockley-Read-Hall recombination centers. It is plausible to assume that these effects also occur at the Ge-NC/SiO_2 interface. Indeed, the experimentally observed size-dependent photoluminescence[5] exhibits a significant redshift as compared to the results of tight-binding calculations for hydrogen passivated Ge NCs.[10] There are different hints that the interface state density for the Ge-NC/SiO_2 interface is much higher than for the Si-NC/SiO_2 interface: (1) for Si nanostructures, efficient size-dependent photoluminescence (PL) attributed to quantum-confinement effects can be obtained.[18–20] For Ge nanocrystals, only a few groups observed size-dependent PL in the near infrared regime,[5,21] which can be attributed to band-to-band transitions in the NCs. By contrast, many researchers reported only a peak at around 2 eV almost independent from the NC size,[4,22,23] which is related to defects in the SiO_2 matrix.[22] The different band to band recombination efficiencies for Si and Ge nanocrystals hints a higher density of interface traps for Ge nanocrystals[24] and/or shorter electron and hole capture times for these traps (as compared to the radiative lifetimes[25]). Both effects would favor nonradiative recombination processes. (2) Koh *et al.*[26] pointed out the importance of traps for the charge storage and retention in Ge nanocrystal memories. One should note that also for Si NC-based memory devices the retention behavior seems to be affected by traps at the nanocrystal/matrix interface.[27] (3) Recent high-resolution transmission electron microscope investigations of the Ge-NC/SiO_2 interface suggest that the crystalline Ge is not directly in contact with the SiO_2 matrix.[28] Rather, the Ge nanocrystals seem to be enclosed by an amorphous Ge layer possibly formed to minimize the interface energy.[28] One should note that similar observations have been reported for Si NCs embedded in SiO_2.[29] Analogously to the *a*-Si/*c*-Si interface, which is known to exhibit a high interface trap density,[30] the same can be expected for the *a*-Ge/*c*-Ge interface.

For all possible fields of application of the Ge-NC:SiO_2 system, the properties of the Ge-NC/SiO_2 interface are im-

portant. While for memory applications a high density of deep level interface states might be advantageous,[26] this would be unfavorable for all optoelectronic applications based on band-to-band transitions since these traps would mediate efficient nonradiative recombination processes.

The aim of this work is the determination of the Ge-NC/SiO_2 interface state density. As compared to an atomistic picture, this is a rather phenomenological quantity. For a certain energy, it can be considered as the sum of all additional states caused by the Ge-NC/SiO_2 interface, which would not be present if the NC would correspond to an ideal potential well, which are localized in the Ge-NC/SiO_2 interface region, and which are accessible for electrons (holes) from the confined states in the conduction (valence) band of the NC. Within this coarse level of description similar to a Shockley-Read-Hall picture, a determination of the physical nature of these states is not necessary. Nevertheless, the knowledge of this quantity would be of great help for the qualitative understanding of different properties of the Ge-NC:SiO_2 system, e.g., the mostly observed absence of efficient size-dependent photoluminescence. So far, there is no report on a quantitative value of the Ge-NC/SiO_2 interface state density. Since the Ge NCs are embedded in SiO_2, the Ge-NC/SiO_2 interface is hardly accessible for surface sensitive investigation methods, e.g., photoemission spectroscopy in the near ultraviolet regime.[31] In this work, we therefore study the properties of the Ge-NC/SiO_2 interface indirectly by analyzing the exchange of electrons between Ge NCs and a Si substrate by charging and discharging processes based on direct tunneling through SiO_2. For these experiments, the NCs are integrated into the gate oxide of metal-oxide-semiconductor (MOS) field-effect transistors. These structures are nanocrystal floating-gate devices,[1] i.e., the NCs are located close enough to the Si substrate so that electrons can pass through the SiO_2 barrier (denoted as tunnel oxide) by direct tunneling. By contrast, the thickness of the SiO_2 between the NCs and the gate electrode (denoted as control oxide) is sufficiently large to suppress tunneling effects. The charge stored in the NCs is altered by a small modulation of the applied gate voltage and its response to the external field is measured as a function of frequency and temperature using the drain current as a sensor. A linearized quantum-mechanical model is used for the interpretation of the results. By this approach, we first calculated the contribution of quantized states in the Ge-NC conduction band to the response of the cluster charge using density-functional theory (DFT). In a second step, we compared this calculated value with the small-signal response extracted from the experiments. Since the latter is possibly affected by the contribution of trap states at the Ge-NC/SiO_2 interface, we estimated the interface trap density from the difference between both values.

The reader should note that the designation of the traps as states at the Ge-NC/SiO_2 interface includes states that can be spatially located in the volume of the nanocrystals, possibly induced by dislocations or other defects.

II. EXPERIMENTAL

A. Sample preparation

The Ge nanoclusters were prepared by a plasma-enhanced chemical vapor deposition-based method described in detail by Dürkop *et al.*[32] In the present work, the nanocrystal preparation was integrated into a standard MOS field-effect transistor fabrication process. In a first step, the tunnel oxide was grown on (100) *p*-type Si wafers by rapid thermal oxidation at 950 °C. Next, an amorphous Ge layer was deposited by plasma-enhanced chemical vapor deposition at 200 °C and *in situ* capped by the control oxide at 400 °C. *In situ* phosphorus doped n^+ polysilicon was used as gate material. The continuous initial Ge layer was transformed into isolated crystalline nanoclusters by self-organization processes during thermal annealing for 7 s at 1000 °C.[28] This annealing step simultaneously activated the implanted dopants in the source/drain regions. A high NC areal density of $\eta=6\times10^{11}$ cm^{-2}, a small average NC radius of $\langle r_{nc}\rangle=2.8$ nm, and low reverse currents for the *pn* junctions were achieved for the chosen annealing parameters. Figure 1 shows a cross section transmission electron microscope (TEM) image of one of the samples. As a last step of device fabrication, the samples were annealed for 30 min at 450 °C in N_2/H_2 atmosphere, i.e., the nanocrystals were exposed to a hydrogen passivation.

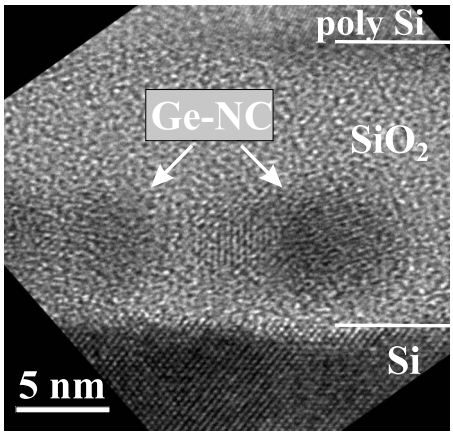

FIG. 1. Cross section TEM image of sample nNC2 (see Table I).

The structural parameters of the samples investigated are listed in Table I. The essential difference between these three samples with *n*-channel MOS transistor test structures of 50 μm gate length and 775 μm effective gate width is the tunnel oxide thickness. In all cases, the small values of $\langle d_{tox}\rangle\leq2.3$ nm ensure efficient charging and discharging processes based on direct tunneling.

B. Measurement method

The electrical characterization of trapping effects at the Ge-NC/SiO_2 interface by a small-signal method has some important advantages as compared to large signal measurements, e.g., performed by Liu *et al.*[33] In case of the latter, the substrate state varies from accumulation to inversion. Therefore, the communication of the NC with the conduction band and the valence band of the substrate has to be taken into account.[34] For small-signal measurements permanently performed in inversion, the consideration can be restricted to the Ge-NC/Si-conduction-band communication. Furthermore,

TABLE I. Structural parameters of the investigated samples determined by TEM and spectral ellipsometry measurements. The substrate doping concentration was extracted from gate to bulk $C(V)$ curves. The maximum error is 0.1 nm for $\langle d_{tox}\rangle$, $\langle d_{cox}\rangle$ and $\langle r_{nc}\rangle$, 2×10^{10} cm^{-2} for η, and 10% of the absolute value for N_A.

Sample	nNC1	nNC2	nNC3
Mean tunnel oxide thickness $\langle d_{tox}\rangle$	1.9 nm	2.1 nm	2.3 nm
Cluster areal density η	6×10^{11} cm^{-2}	6×10^{11} cm^{-2}	6×10^{11} cm^{-2}
Mean NC radius $\langle r_{nc}\rangle$	2.8 nm	2.8 nm	2.8 nm
Mean control oxide thickness $\langle d_{cox}\rangle$	10.3 nm	10.3 nm	10.4 nm
Substrate doping concentration N_A	9.8×10^{15} cm^{-3}	1.6×10^{15} cm^{-3}	5.7×10^{15} cm^{-3}

the electrostatic field distribution in the sample is not altered strongly during the small-signal measurements. Due to this, essential simplifications in the theoretical description are justified (see below).

In order to characterize the linear response of the total charge Q_{nc} stored within the nanocrystals to a small variation of the gate voltage, a small ac signal $\underline{v}_{GB}$ is superimposed on a relatively large dc component V_{GB0} of the gate voltage [Fig. 2(a)]. (In the following, the quantities exhibiting a harmonic oscillation are underlined since they can be considered as complex numbers.) If exclusively V_{GB0} would be applied, there would be a stationary amount of charge Q_{nc}^0 stored within the NCs after a sufficiently long charging time corresponding to a saturation flat-band voltage V_{FB0}. The value of Q_{nc}^0 is determined by the total density of states in the NC and at the Ge/SiO_2 interface and by the position of the quasi-Fermi level in the NC. For the samples investigated, the substrate is under weak inversion in this stationary state.

Due to the small oscillating component $\underline{v}_{GB}$ of the gate voltage, Q_{nc} is slightly altered by the exchange of electrons between the NCs and the Si conduction band due to emission and capture processes. The measured quantity is the small-signal modulation $\underline{i}_D$ of the drain current. It strongly depends on the frequency-dependent response of the NCs to the ac part of the gate voltage [Fig. 2(b)]. For very low frequencies, charging, and discharging processes are able to follow the alternations of $\underline{v}_{GB}$. The cluster charge increases slightly during the first half of the period and decreases slightly during the second half of the period, i.e., $Q_{nc}=Q_{nc}^0+\underline{q}_{nc}$. Therefore, the channel itself is partially screened from the ac signal by the corresponding alternation of the flat-band voltage $V_{FB}=V_{FB0}+\underline{v}_{FB}$ and the modulation of the drain current is small. For very high frequencies, the charging and discharging processes are not able to follow the ac part of the gate voltage. Therefore, Q_{nc} and V_{FB} are not altered and the channel can be modulated by $\underline{v}_{GB}$ according to the frequency independent transconductance g_m^∞ of the MOS transistor. The reader should note that the modulation of the drain current is largely dominated by the small-signal alternation of the electrostatic field distribution induced by $\underline{v}_{GB}$ while the contribution of the tunnel current between the NCs and the substrate is negligible. In the intermediate frequency regime, a phase shift between $\underline{i}_D$ and $\underline{v}_{GB}$ is observed (Fig. 2). The frequency dependence of the modulation of the drain current can be expressed by a complex transconductance $\underline{g}_m(f)\equiv\underline{i}_D/\underline{v}_{GB}=|\underline{g}_m|\exp(i\varphi_{\underline{g}_m})$.

Since the devices investigated contain a high number of $\approx2\times10^8$ nanocrystals, the following charge-sheet approximation should hold:[35]

$$Q_{nc}=-e\eta\langle N\rangle\simeq-C_{cox}(V_{FB}-\Phi_{ms}). \tag{1}$$

Here, $\langle N\rangle$ denotes the ensemble averaged number of electrons stored in one nanocrystal at a certain point in time, $C_{cox}\simeq\varepsilon_0\varepsilon_r^{SiO_2}(\langle d_{cox}\rangle+1/2\varepsilon_r^{SiO_2}/\varepsilon_r^{Ge}\langle d_{nc}\rangle)^{-1}$ denotes the capacitance between the ensemble of NCs and the control gate, e denotes the elementary charge, and Φ_{ms} denotes the work function difference between the control gate and the substrate. The relative dielectric constants of Ge and SiO_2 are denoted by ε_r^{Ge} and $\varepsilon_r^{SiO_2}$, respectively. Within a first-order approximation of the drain current $I_D(V_{GB},V_{FB})$ at (V_{GB0},V_{FB0}), it can easily be shown from Eq. (1) that the small-signal variations in the cluster charge and of the gate voltage are related by

$$\chi_{nc}(f)\equiv-\left.\frac{\underline{q}_{nc}}{\underline{v}_{GB}}\right|_{V_{GB0}}\simeq C_{cox}\left[1-\frac{\underline{g}_m(f)}{g_m^\infty}\right]. \tag{2}$$

In the following, the quantity χ_{nc} is denoted as the frequency-dependent susceptibility of the charge stored in the nanocrystals. One should note that the normalized sus-

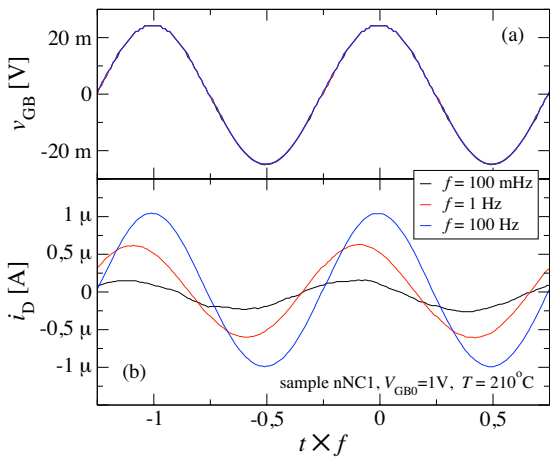

FIG. 2. (Color online) Illustration of the measurement method: (a) a small ac component is superimposed on a large dc component $V_{GB0}=1$ V of the gate voltage. (b) Corresponding modulation of the drain current reflecting the frequency dependence of the response of the cluster charge to the alternating field (sample nNC1, $V_{DB}=0.1$ V, and $T=210$ °C).

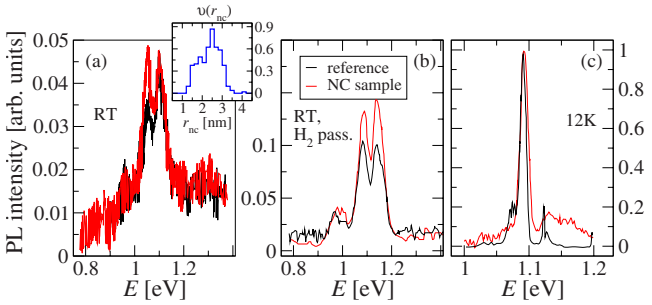

FIG. 3. (Color online) (a) Comparison of the room-temperature photoluminescence spectra of a sample with Ge-NCs embedded in SiO_2 with a reference sample with a pure SiO_2 layer on Si substrate. The inset shows the NC size distribution determined by TEM. (b) Room-temperature PL spectra of the samples shown in (a) obtained after 30 min N_2/H_2 annealing at 400 °C. (c) Spectra of both samples at 12 K.

ceptibility χ_{nc}/C_{cox}, which is the quantity actually measured in our experiments, is not an intrinsic property of the Ge-NC:SiO_2 system (see below). Rather, it depends on device parameters such as the tunnel oxide thickness and has therefore to be considered as an effective susceptibility.

By comparing the value of the frequency-independent transconductance g_m^∞ with the transfer characteristic of the device,[34] the value of the stationary flat-band voltage V_{FB0} was obtained. The exponential relation between g_m^∞ and V_{FB0} in the subthreshold regime ensures a very high sensitivity of this determination method, and thus a small maximum error ≤ 25 mV.

An *Agilent 33250 A* function generator was used to provide the gate voltage, while a constant drain voltage of $V_{DB}=0.1$ V was applied by a *Keithley 230* voltage source. The small value of V_{DB} ensured a small potential drop across the channel and therefore laterally uniform charging and discharging processes. The transient drain current was measured by a fast *FEMTO DHCPA-100* current-voltage converter and an *Agilent DSO 6062A* oscilloscope. Fast Fourier transformation was used to extract the amplitude of and the phase shift between $\underline{i}_D$ and $\underline{v}_{GB}$ from the digitalized signal.

C. Photoluminescence measurements

Supplementary to the electrical characterization described above, we performed photoluminescence measurements in order to obtain additional information about the importance of trap states at the Ge-NC/SiO_2 interface. If the trap density were sufficiently low, one would expect a significant peak in the near infrared regime at ≈ 0.8 eV for our value of $\langle r_{nc} \rangle = 2.8$ nm.[5] This peak could be attributed to band-to-band transitions in the Ge-NCs. The PL measurements were performed on unstructured Ge-NC/SiO_2 samples exhibiting the same cluster areal density and size as the MOS transistor samples (equal NC formation process step). The excitation was performed by a GaN laser at 405 nm with a power of 14 mW at the sample. The PL spectra were acquired by a double grating monochromator and a *Hamamatsu 1998* photomultiplier. Figure 3(a) shows the PL spectra of a sample with Ge-NCs embedded in SiO_2 and of a reference sample with a pure SiO_2 layer on a Si substrate. As shown in the inset, a large fraction of the nanocrystals exhibits a radius smaller than 2.8 nm. According to Takeoka *et al.*,[5] the band-to-band transitions in these NCs should be located in the measured energy interval (≥ 0.8 eV). The large areal density of the NCs should be sufficient for the detection of this luminescence. However, the spectrum of the sample containing Ge NCs is identical to that of the reference sample without any clusters. The two peaks visible in the spectra arise from the TO phonon-mediated transition at 1.09 eV and from the band-to-band transition at 1.12 eV in the Si substrate. No luminescence attributable to the Ge NCs can be resolved. An additional hydrogen passivation of the samples (at 400 °C in N_2/H_2) increases the PL intensity, but does not alter the shape of the spectra [Fig. 3(b)]. Also, in a low temperature measurement at 12 K, no luminescence attributable to the Ge NCs can be resolved [Fig. 3(c)]. One should note that at 12 K, the Ge band gap is increased to 0.74 eV. Therefore, a possible luminescence of almost all NCs can be expected to contribute to the spectra within the energy interval considered.[5] The absence of any PL attributable to the Ge NCs strongly indicates efficient nonradiative recombination processes in the nanocrystals, which can be expected to be mediated by trap states with a high density. According to this picture, one can estimate an upper limit for the time scales of capture of charge carriers from the quantized cluster states by the traps. The capture time should be smaller than the radiative recombination lifetime, which is in the range of $10^{-3}-10^{-2}$ s.[25]

III. MODELING

In previous works, an idealized system without any traps at the Ge/SiO_2 interface has been considered within a three-dimensional quantum-mechanical picture.[36,37] In the following, we present a small-signal expansion of this approach considering the system to be in a stationary state while a small perturbation of the electrostatic field distribution is superimposed. This ansatz takes into account the presence of Ge-NC/SiO_2 interface states in the band gap of the nanocrystal. The small-signal expansion yields simple analytical expressions which can be used to extract an important parameter from the measured spectra of $\chi_{nc}(f)$, which we denoted by α (see below). This quantity describes the derivative of the charge stored in the NC with respect to the position of the quasi-Fermi level in the nanocrystal and thus depends on the total density of states of the NC. It can also be calculated theoretically by density-functional theory for an ideal system without any traps. From a comparison of both values, the contribution of trap states at the Ge-NC/SiO_2 interface can be extracted.

Our model is based on the following assumptions (Fig. 4): (i) the small-signal behavior can be described within a continuum picture. The modulation of the average charge per NC can exhibit small fractional values of e. This assumption is motivated by the huge number of $\approx 2\times 10^8$ nanocrystals per device. Because of this, an ensemble-averaged modulation of the cluster charge is sensed. Statistically, only some of the NCs are exchanging charge carriers with the substrate,

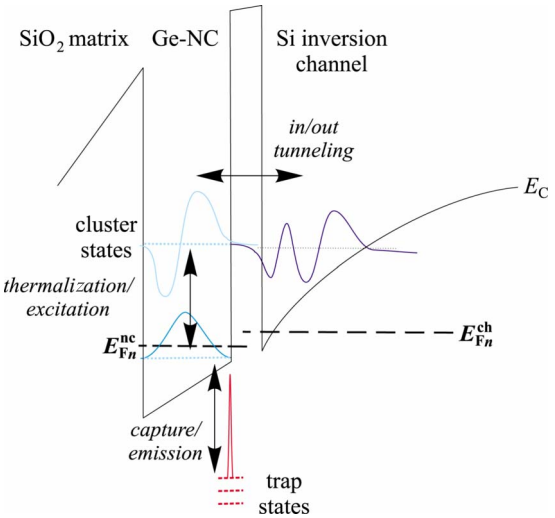

FIG. 4. (Color online) Illustration of the basic assumptions made for the small-signal expansion. Only the quantized cluster states exchange electrons with the states in the channel. The trap states at the Ge-NC/SiO_2 interface and the quantized cluster states are in equilibrium with each other and can therefore be described by one quasi-Fermi level E_{Fn}^{nc}. Due to the alternating part of the gate voltage, E_{Fn}^{nc} is slightly shifted with respect to E_{Fn}^{ch}.

depending on the respective positions of the quasi-Fermi levels. Coulomb blockade effects are assumed to be negligible, at least for the measurement temperatures ≥ 300 K. (ii) The charge carrier exchange between the nanocrystal and the substrate is dominated by the communication between the quantized cluster states and the Si conduction band, while the direct communication between the Ge-NC/SiO_2 interface states and the Si conduction band plays a minor role. This assumption can be justified by the argument that the electron wave functions corresponding to the quantized states within the conduction band of the NCs are much more extended in space than the electron wave functions corresponding to the Ge-NC/SiO_2 interface states. Therefore, the overlap with the electron wave functions in the channel is much stronger for the NC states, and the respective transition rate is much larger. (iii) The quantized states in the conduction band of the NC and the Ge-NC/SiO_2 interface states in the band gap of the NC are in equilibrium with each other and can therefore be described by the same quasi-Fermi level. This assumption is based on the following arguments: The small band gap of Ge implies small time constants for the capture (emission) of an electron from (to) the Ge conduction band by the interface states. On the other hand, relatively large time constants are implied for the exchange between the NC and the Si conduction band due the tunnel distance and the small voltage drop across the tunnel oxide in the stationary state. Therefore, the latter process is much slower and thus dominates the charging and discharging dynamics. (iv) The presence of localized, possibly occupied trap states is not strongly affecting the energy eigenvalues of the confined states in the conduction band of the NC. In other words, we expect the density of confined cluster states in the real system, where traps are present, not to differ by orders of magnitude from that in an ideal system without any traps. This is probably the most questionable assumption since even a single trap state present at the interface of a NC is known to significantly affect its overall electronic structure.[38] However, we are only interested in the order of magnitude of the density of the quantized cluster states in order to calculate their contribution to the parameter α. One should note that an exact calculation of the energy eigenvalues and eigenfunctions in the NC conduction band is impossible for the real Ge-NC:SiO_2 system because the spatial positions and the physical nature of the trap states are not known.

These assumptions enable us to calculate the charging and discharging dynamics of the nonideal system including Ge-NC/SiO_2 interface traps analogously to the idealized system,[36,37] i.e., restricting the consideration to transitions between the quantized states within the NC and the channel. In this picture, the tunnel current from the channel into one nanocrystal is given by[36,39]

$$J_{\mathrm{ch}\rightarrow\mathrm{nc}}^{1\ \mathrm{nc}} = 2e \sum_{\mathrm{ch\ valley}} \sum_{\mathrm{nc\ valley}} \left(\sum_m \sum_n \frac{1}{\tau_{m,n}} \right), \tag{3}$$

where the contribution of every possible transition between the electron states in the mth conduction subband in the channel and the nth quantized states in the nanocrystal as well as all equivalent valleys in the Si substrate and in the Ge NC are taken into account. The additional factor 2 accounts for spin degeneracy. The individual transition rates are given by[36]

$$\frac{1}{\tau_{m,n}} = \frac{2\pi}{\hbar} \sum_{veck_\parallel} |M_{m,n}|^2 f_{2\mathrm{D}}(E_m, E_{Fn}^{\mathrm{ch}}) \times [1 - f_{0\mathrm{D}}(E_n, E_{Fn}^{\mathrm{nc}})] \delta(E_m - E_n) \tag{4}$$

In Eq. (4), $f_{0\mathrm{D}}$ and $f_{2\mathrm{D}}$ are the Fermi-Dirac occupation distributions of electrons in the cluster and in the channel depending on the respective quasi-Fermi level E_{Fn}^{nc} and E_{Fn}^{ch}. The summation is carried out over all transverse wave vectors $\vec{k}_\parallel$ in the two-dimensional (2D) channel. The coupling matrix element $M_{m,n}$ can be calculated according to Bardeen's formalism by[36]

$$M_{m,n} = -\frac{\hbar^2}{2m^\star} \int_\Omega [\psi_m^\star \nabla \psi_n - \psi_n \nabla \psi_m^\star] d^2 r. \tag{5}$$

Here, ψ_n and ψ_m denote the electron wave functions in the nanocrystal and in the channel. The integration is performed over an arbitrary surface Ω lying in a plane parallel to the Si/SiO_2 interface within the tunnel barrier. In order to calculate the net current density J^{total} between all NCs and the substrate, the reverse current from the nanocrystals into the substrate has to be subtracted. Within Harrison's independent tunneling model[40] under the constraint of transverse momentum conservation the net current density is given by[39]

$$J^{\mathrm{total}} = \frac{4\pi e \eta}{\hbar} \sum_{\mathrm{ch\ valley}} \sum_{\mathrm{nc\ valley}} \sum_m \sum_n \sum_{\vec{k}_\parallel} |M_{m,n}|^2 [f_{2\mathrm{D}}(E_m, E_{Fn}^{\mathrm{ch}}) - f_{0\mathrm{D}}(E_n, E_{Fn}^{\mathrm{nc}})] \delta(E_m - E_n). \tag{6}$$

A. Small-signal expansion

So far, the equations also account for the large-signal behavior. For small perturbations, they can be simplified as follows: The small variation in the gate voltage alters the electrostatic field distribution insignificantly. Therefore, the tunnel barrier, coupling matrix elements $M_{m,n}$, the energy eigenvalues $E_{m(n)}$, and the eigenstates $\psi_{m(n)}$ can be considered as constant. The tunneling current induced by the ac part of the gate voltage is mainly caused by a small variation of the positions of the quasi-Fermi levels in the NC and in the substrate. Within a first-order Taylor expansion, the positions of the quasi-Fermi levels are given by

$$f_{2\mathrm{D}}(E_m,E_{Fn}^{\mathrm{ch}}) \simeq f_{2\mathrm{D}}(E_m,E_{Fn}^{\mathrm{ch},0}) + \left.\frac{\partial f_{2\mathrm{D}}}{\partial E_{Fn}^{\mathrm{ch}}}\right|_{E_{Fn}^{\mathrm{ch},0}} \Delta E_{Fn}^{\mathrm{ch}},$$

$$f_{0\mathrm{D}}(E_n,E_{Fn}^{\mathrm{nc}}) \simeq f_{0\mathrm{D}}(E_n,E_{Fn}^{\mathrm{nc},0}) + \left.\frac{\partial f_{0\mathrm{D}}}{\partial E_{Fn}^{\mathrm{nc}}}\right|_{E_{Fn}^{\mathrm{nc},0}} \Delta E_{Fn}^{\mathrm{nc}}. \quad (7)$$

In the stationary state (absence of the ac signal), there is no net current flowing between the nanocrystals and the substrate. In this case, the NCs and the Si substrate are in equilibrium with each other, corresponding to coinciding quasi-Fermi levels $E_{Fn}^{\mathrm{ch},0}=E_{Fn}^{\mathrm{nc},0}\equiv E_F^0$. Inserting Eq. (7) into Eq. (6) yields a first-order approximation of the tunneling current $\underline{j}^{\mathrm{total}} \simeq J^{\mathrm{total},0}+\underline{j}^{\mathrm{total}}$, where the constant part $J^{\mathrm{total},0}$ is zero due to the equality of the quasi-Fermi levels in the stationary state. The oscillating part $\underline{j}^{\mathrm{total}}$ is given by

$$\underline{j}^{\mathrm{total}} = \frac{4\pi e\,\eta}{\hbar} \sum_{\mathrm{ch}} \sum_{\mathrm{valley\,nc}} \sum_{\mathrm{valley}} \sum_{m} \sum_{n} \sum_{\vec{k}_{\parallel}} |M_{m,n}|^2 \times \frac{\exp\left(\frac{E_n - E_F^0}{k_{\mathrm{B}}T}\right)}{k_{\mathrm{B}}T\left[1+\exp\left(\frac{E_n - E_F^0}{k_{\mathrm{B}}T}\right)\right]^2} \delta(E_m - E_n) \times [\Delta E_{Fn}^{\mathrm{nc}} - \Delta E_{Fn}^{\mathrm{ch}}], \quad (8)$$

$$\equiv g\frac{1}{e}[\Delta E_{Fn}^{\mathrm{nc}} - \Delta E_{Fn}^{\mathrm{ch}}]. \quad (9)$$

The quantity g can be considered as a small-signal conductance independent of the frequency. The frequency dependence of $\chi_{\mathrm{nc}}(f)$ is related to the frequency dependent difference $[\Delta E_{Fn}^{\mathrm{nc}} - \Delta E_{Fn}^{\mathrm{ch}}]$ between the quasi-Fermi levels. It will be derived in the following.

For the total charge Q_{nc} stored in the nanocrystals and for the charge Q_s induced in the silicon substrate, a first-order approximation yields

$$Q_{\mathrm{nc}}(E_{Fn}^{\mathrm{nc}}) \simeq Q_{\mathrm{nc}}^0(E_F^0) + \left.\frac{dQ_{\mathrm{nc}}}{dE_{Fn}^{\mathrm{nc}}}\right|_{E_F^0} \Delta E_{Fn}^{\mathrm{nc}} \equiv Q_{\mathrm{nc}}^0 + \underline{q}_{\mathrm{nc}}, \quad (10)$$

$$Q_s(E_{Fn}^{\mathrm{ch}},\varphi_s) \simeq Q_s^0(E_F^0,\varphi_s^0) + \left.\frac{\partial Q_s}{\partial E_{Fn}^{\mathrm{ch}}}\right|_{E_F^0,\varphi_s^0} \Delta E_{Fn}^{\mathrm{ch}} + \left.\frac{\partial Q_s}{\partial \varphi_s}\right|_{E_F^0,\varphi_s^0} \Delta\underline{\varphi}_s \equiv Q_s^0 + \underline{q}_s. \quad (11)$$

In Eq. (11), φ_s denotes the surface potential in the Si substrate, φ_s^0 its value in the stationary state, and $\Delta\underline{\varphi}_s$ its small variation induced by the ac part of the gate voltage. Rearranging Eqs. (10) and (11) yields the difference between the quasi-Fermi levels

$$\Delta E_{Fn}^{\mathrm{nc}} - \Delta E_{Fn}^{\mathrm{ch}} = \frac{\underline{q}_{\mathrm{nc}}}{\alpha} - \frac{\underline{q}_s}{\beta} + \frac{C_s\Delta\underline{\varphi}_s}{\beta}. \quad (12)$$

The constant parameters $\beta \equiv \partial Q_s/\partial E_{Fn}^{\mathrm{ch}}|_{E_F^0,\varphi_s^0}$ and $C_s \equiv \partial Q_s/\partial\varphi_s|_{E_F^0,\varphi_s^0}$ can be calculated analytically using standard MOS equations. By contrast, the parameter $\alpha \equiv dQ_{\mathrm{nc}}/dE_{Fn}^{\mathrm{nc}}|_{E_F^0}$ contains an unknown contribution of the Ge-NC/SiO_2 interface states and requires further discussion. In general, the total cluster charge can be divided into the fraction of charge carriers stored in the quantized cluster states and the fraction of charge carriers stored in the trap states, i.e.,

$$Q_{\mathrm{nc}} = \underbrace{-e\sum_n f_{0\mathrm{D}}(E_n,E_{Fn}^{\mathrm{nc}})}_{Q_{\mathrm{nc}}^{\mathrm{ideal}}} \underbrace{-e\int_{E_{NP}}^{\infty} N_{\mathrm{it}}(E) f_{0\mathrm{D}}(E,E_{Fn}^{\mathrm{nc}})dE}_{Q_{\mathrm{it}}}. \quad (13)$$

In the second term of Eq. (13), integration is used since the trap states can be expected to exhibit a continuous energy distribution in terms of ensemble averaged properties. The density of Ge-NC/SiO_2 interface states is denoted by N_{it}. The lower integration limit corresponds to the charge neutrality level E_{NP} of the traps. In Eq. (13), possibly unoccupied trap states with an energy below E_{NP}, which would be positively charged, are neglected. Furthermore, the even more fundamental interaction between the (occupied) density of trap states and the quantized cluster states is neglected [assumption (iv)]. Using Eq. (13), α can be partitioned into

$$\alpha = \left.\frac{dQ_{\mathrm{nc}}^{\mathrm{ideal}}}{dE_{Fn}^{\mathrm{nc}}}\right|_{E_F^0} + \left.\frac{dQ_{it}}{dE_{Fn}^{\mathrm{nc}}}\right|_{E_F^0} \approx \alpha_{\mathrm{nc}}^{\mathrm{ideal}} - eN_{\mathrm{it}}(E_F^0). \quad (14)$$

The second term in Eq. (14) was obtained by the approximation $f_{0\mathrm{D}}(E,E_F^0) \approx 1-\Theta(E-E_F^0)$, where Θ denotes the Heaviside function. As already mentioned above, the density N_{it} of Ge-NC/SiO_2 interface states in the vicinity of E_F^0 can be obtained by subtracting the calculated value of $\alpha_{\mathrm{nc}}^{\mathrm{ideal}}$ from the value of α extracted from the experiments. The oscillating part $\underline{q}_s$ of the charge induced on the silicon substrate can be related to the voltage balance of the small-signal components

$$\underline{v}_{\mathrm{GB}} = \frac{-\underline{q}_s}{C_{\mathrm{ox}}} + \Delta\underline{\varphi}_s - \frac{\underline{q}_{\mathrm{nc}}}{C_{\mathrm{ox}}}, \quad (15)$$

where C_{ox} denotes the total oxide capacitance. Assuming a harmonic modulation $\underline{q}_{\mathrm{nc}}=\hat{q}_{\mathrm{nc}}\exp[i(\omega t-\vartheta)]$ of the cluster

charge, the left-hand side of Eq. (12) can be replaced by

$$\Delta E_{Fn}^{\mathrm{nc}} - \Delta E_{Fn}^{\mathrm{ch}} = \frac{e}{g}\underline{j}^{\mathrm{total}} = \frac{e}{g}\frac{d\underline{q}_{\mathrm{nc}}}{dt} = i\omega\underline{q}_{\mathrm{nc}}\frac{e}{g}. \tag{16}$$

Inserting Eqs. (15) and (16) in Eq. (12) yields

$$i\omega\frac{e}{g}\underline{q}_{\mathrm{nc}} = \frac{\underline{q}_{\mathrm{nc}}}{\alpha} + \frac{C_{\mathrm{ox}}}{\beta}\underline{v}_{\mathrm{GB}} + \frac{C_{\mathrm{ox}}}{\beta C_{\mathrm{cox}}}\underline{q}_{\mathrm{nc}} - \frac{1}{\beta}(C_{\mathrm{ox}} - C_s)\Delta\underline{\varphi}_s. \tag{17}$$

Since the surface potential in the silicon substrate only weakly depends on the gate voltage in the state of inversion (stationary state), its variation $\Delta\underline{\varphi}_s$ can be neglected. Then, one obtains the following theoretical expression for the susceptibility $\chi_{\mathrm{nc}} = -\underline{q}_{\mathrm{nc}}/\underline{v}_{\mathrm{GB}}$:

$$\chi_{\mathrm{nc}} = \frac{C_{\mathrm{ox}}}{\frac{C_{\mathrm{ox}}}{C_{\mathrm{cox}}} + \frac{\beta}{\alpha} - \frac{i\omega\beta e}{g}}. \tag{18}$$

As we will discuss in Sec. IV, Eq. (18) can be used to extract the parameters α and g from the experimental spectrum of $\chi_{\mathrm{nc}}(f)$.

B. Contribution of the quantized cluster states

For the calculation of the theoretical values of g and of $\alpha_{\mathrm{nc}}^{\mathrm{ideal}}$, we use a three-dimensional quantum-mechanical model described in detail in previous works.[36] Briefly summarized, the eigenvalues $E_{m(n)}$ and the eigenstates $\psi_{m(n)}$ are obtained by self-consistent solution of the Poisson equation

$$\nabla\cdot[\varepsilon_0\varepsilon_r(\vec{r})\,\nabla\,\varphi(\vec{r})] = -e[p(\vec{r}) - n(\vec{r}) - N_A^-(\vec{r})] \tag{19}$$

and the Kohn-Sham equation

$$\left[-\frac{\hbar^2}{2}\nabla\, m^{-1}(\vec{r})\,\nabla - e\varphi(\vec{r}) + V_{xc}(\vec{r}) + \Delta E_C(\vec{r})\right]\psi_i(\vec{r}) = E_i\psi_i(\vec{r}) \tag{20}$$

in a three-dimensional simulation box containing one Ge NC with $r_{\mathrm{nc}} = \langle r_{\mathrm{nc}}\rangle$. Here, $p(\vec{r})$, $n(\vec{r})$, and $N_A^-(\vec{r})$ denote the position-dependent hole, electron, and ionized impurity densities in the Si substrate. Furthermore, $\varepsilon_0\varepsilon_r(\vec{r})$ denotes the dielectric constant and $m(\vec{r})$ denotes the effective mass, both depending on $\vec{r}$. The position-dependent conduction band offset between materials is denoted by $\Delta E_C(\vec{r})$. The exchange-correlation potential $V_{xc}(\vec{r})$ is obtained within the local density approximation of the DFT. The potential distribution was calculated for a number N of electrons per cluster, which was chosen as the nearest integer value to the experimental value $\langle N\rangle$ obtained from V_{FB0} according to Eq. (1). For $V_{\mathrm{GB0}} = 1$ V, approximately three electrons were stored per nanocrystal in the stationary state. Once $E_{m(n)}$ and $\psi_{m(n)}$ were known, $M_{m,n}$ and subsequently g were calculated according to Eqs. (5) and (8). The contribution of the quantized cluster states to α was calculated according to

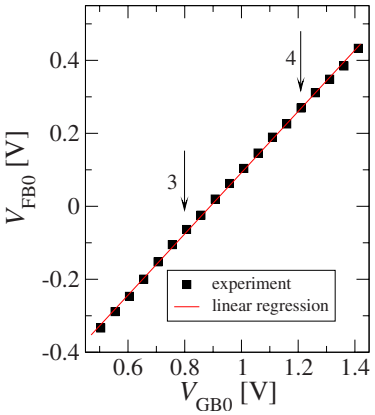

FIG. 5. (Color online) Saturation flat-band voltage V_{FB0} as a function of the dc part V_{GB0} of the gate voltage (sample nNC1 and 25 °C). The arrows indicate V_{GB0} values which yield an integer number $\langle N\rangle = Q_{\mathrm{nc}}^0/(\eta e)$ of electrons stored per nanocrystal (within the framework of the charge-sheet approximation [Eq. (1)]). V_{DB} was fixed at 0.1 V and $\hat{v}_{\mathrm{GB}}$ was 25 mV.

$$\alpha_{\mathrm{nc}}^{\mathrm{ideal}} = \frac{-e}{\delta E}\sum_n f_{0\mathrm{D}}(E_n, E_F^0 + \delta E) - f_{0\mathrm{D}}(E_n, E_F^0) \tag{21}$$

using a sufficiently small value of δE. In the simulations, the measurement temperature T affects the position of the Fermi level in the Si substrate as well as the carrier concentrations entering in Eq. (19). The band gap narrowing with increasing T is also taken into account. However, in the DFT calculations $T = 0$ K is assumed.

IV. RESULTS AND DISCUSSION

First, we checked the validity of assumption (i). As shown in Fig. 5, an increase of the dc part of the gate voltage yields an almost linear increase of the saturation flat-band voltage although the small incremental steps of V_{GB0} of 25 mV imply fractional changes in the average number of electrons $\langle N\rangle = Q_{\mathrm{nc}}^0/(\eta e)$ stored per NC [Eq. (1)]. Thus, the small-signal response of the cluster charge can be described within a continuum picture, at least for measurement temperatures equal to or larger than room temperature. However, Coulomb blockade effects may occur at much lower temperatures,[41] yielding plateau values in $V_{\mathrm{FB0}}(V_{\mathrm{GB0}})$ with a width of ≈ 130 mV.[42]

Figure 6(a) shows the temperature behavior of the susceptibility $\chi_{\mathrm{nc}}(f) \equiv -\underline{q}_{\mathrm{nc}}/\underline{v}_{\mathrm{GB}}$ for sample nNC1, measured at $V_{\mathrm{GB0}} = 1$ V. Especially at higher temperatures, the remarkable features of the spectra are visible within the measurement range 10 mHz $\leq f \leq$ 1 kHz: The real part of χ_{nc} exhibits a plateau for small frequencies. With increasing frequency, $\mathrm{Re}\{\chi_{\mathrm{nc}}(f)\}/C_{\mathrm{cox}}$ decreases to zero. This behavior can be understood intuitively. For very small frequencies, the small alternating signal $\underline{v}_{\mathrm{GB}}$ causes an alternation of the cluster charge with a constant amplitude. For higher frequencies, the charging and discharging processes are not longer able to follow the oscillations of the external field. Thus, the cluster charge becomes less sensitive to $\underline{v}_{\mathrm{GB}}$. The plateau value of $\mathrm{Re}\{\chi_{\mathrm{nc}}(f\to 0)\}/C_{\mathrm{cox}} \simeq 0.9$ indicates a large, but finite, total

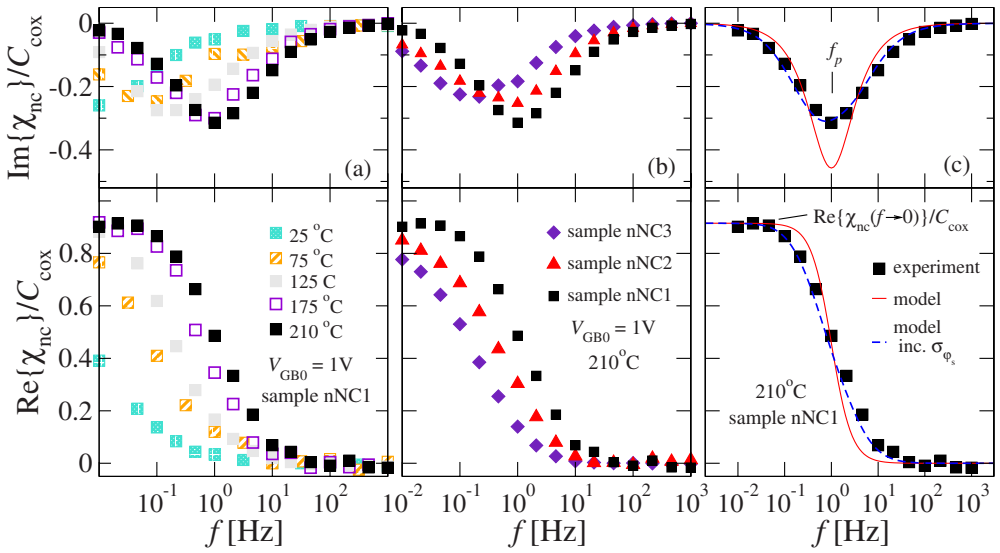

FIG. 6. (Color online) Measured normalized real and imaginary part of the effective susceptibility as a function of frequency. (a) Temperature dependence of $\chi_{nc}(f)$ for sample 1 ($V_{GB0}=1$ V). (b) Comparison of $\chi_{nc}(f)$ for different tunnel oxide thicknesses for 210 °C and $V_{GB0}=1$ V. (c) Comparison of the experimental data (symbols, corresponding to sample 1, 210 °C, and $V_{GB0}=1$ V) and the theoretical behavior of $\chi_{nc}(f)$ according to Eq. (18) (solid lines). The parameters α and g used in the calculation were extracted from the experimental data (Table II). The dashed lines represent the calculated behavior of $\chi_{nc}(f)$ when a small fluctuation of the surface potential φ_s^0 is taken into account. In all measurements, V_{DB} was fixed at 0.1 V, and $\hat{v}_{GB}$ was 25 mV.

density of states in the nanocrystal. In the limiting case of an infinite density of states, the alternation of the cluster charge would totally screen the channel from the ac signal, yielding $\underline{i}_D(f\to 0)=0$, $\underline{g}_m(f\to 0)=0$, and $\mathrm{Re}\{\chi_{nc}(f\to 0)\}/C_{cox}=1$. For $f\to 0$, the modulation of the cluster charge is in phase with $\underline{v}_{GB}$ and thus the imaginary part of χ_{nc} is zero. For increasing frequency, a phase shift between $\underline{q}_{nc}$ and $\underline{v}_{GB}$ occurs, yielding an increasing imaginary part of χ_{nc}. For very high frequencies, the absolute value of χ_{nc} tends to zero. Therefore, $\mathrm{Im}\{\chi_{nc}(f)\}/C_{cox}$ vanishes while the phase of χ_{nc} remains constant at $\pi/2$. With increasing temperature, the spectra shift to higher frequencies. Furthermore, the shape of the spectra changes: the decrease in the real part of χ_{nc} from the plateau value $\mathrm{Re}\{\chi_{nc}(f\to 0)\}/C_{cox}$ to zero steepens for higher temperatures while the peak in the imaginary part narrows and increases in height. The temperature shift of the spectra of χ_{nc} can mainly be attributed to the intrinsic temperature dependence of the small-signal conductance g. This parameter, which essentially determines the frequency range within which the charge stored in the NCs is able to respond to the alternating electrical field, exhibits an almost exponential temperature dependence (see below). An alternative explanation would be that assumption (ii) is not valid, i.e., that the Ge-NC/SiO_2 interface states can directly exchange electrons with the Si conduction band. The temperature shift of the spectra of χ_{nc} could then be attributed to a thermally activated detrapping. However, from the excellent agreement between the experimentally extracted values of g and those calculated according to Eq. (8) (see below), we can exclude this possibility.

Figure 6(b) compares the measured spectra of the susceptibility $\chi_{nc}(f)$ for sample nNC1, nNC2, and nNC3. As expected, the frequency range within which the cluster charge is able to respond to the alternating signal shifts to lower values with increasing tunnel-oxide thickness. This observation sustains our basic assumption (iii) that the quantized states in the conduction band of the NCs and the Ge-NC/SiO_2 interface states are in equilibrium with each other, at least for the measurement temperature of 210 °C. Otherwise, i.e., if a detrapping of the electrons from the interface states into the quantized states in the conduction band

TABLE II. Temperature dependence of the measured small-signal parameters of sample nNC1 for $V_{GB0}=1$ V. The value of β was calculated from standard MOS equations using the measured value of V_{FB0}. The maximum error is 0.05 for $\mathrm{Re}\{\chi_{nc}(f\to 0)\}/C_{cox}$, 5% of the absolute value for f_p, and 20 mV for V_{FB0}. (Superscript † shows extrapolated.)

	25 °C	75 °C	125 °C	175 °C	210 °C
V_{FB0} (V)	0.14	0.25	0.33	0.34	0.44
$\mathrm{Re}\{\chi_{nc}(f\to 0)\}/C_{cox}$	$0.9^{\dagger}$	$0.9^{\dagger}$	0.905	0.92	0.915
$\mathrm{Im}\{\chi_{nc}(f_p)\}/C_{cox}$	−0.25	−0.25	−0.28	−0.3	−0.315
f_p (Hz)	$0.01^{\dagger}$	0.08	0.15	0.8	1
β (As m^{-2} eV^{-1})	-8.811×10^{-5}	-1.316×10^{-4}	-3.283×10^{-4}	-1.28×10^{-3}	-1.957×10^{-3}

TABLE III. Experimental, extracted, and theoretical parameters of samples nNC2 and nNC3 for 210 °C and $V_{GB0}=1$ V. (Superscript † shows extrapolated.)

Sample	nNC2	nNC3
V_{FB0} (V)	0.508	0.576
$\mathrm{Re}\{\chi_{nc}(f\rightarrow 0)\}/C_{cox}$	$0.9^{\dagger}$	$0.9^{\dagger}$
$\mathrm{Im}\{\chi_{nc}(f_p)\}/C_{cox}$	−0.25	−0.235
f_p (Hz)	0.9	0.15
α_{total} (As m^{-2} eV^{-1})	-6.5×10^{-2}	-2.3×10^{-2}
β (As m^{-2} eV^{-1})	-5.82×10^{-3}	-1.98×10^{-3}
g (S m^{-2})	2.4×10^{-2}	2.16×10^{-3}
α_{nc}^{ideal} (As m^{-2} eV^{-1}) (two electrons per NC)	7.523×10^{-4}	7.574×10^{-4}
α_{nc}^{ideal} (As m^{-2} eV^{-1}) (three electrons per NC)	6.792×10^{-4}	6.890×10^{-4}

of the NC would limit the time scales for charging and discharging, one would expect the behavior of χ_{nc} to be independent of the tunnel oxide thickness.[33] The peak in the spectra of the imaginary part seems to broaden with increasing tunnel-oxide thickness while its height seems to decrease. Possible mechanisms explaining this behavior are discussed below.

Figure 6(c) compares the measured behavior of $\chi_{nc}(f)$ (symbols) with the spectrum calculated according to Eq. (18) (solid line). There is an excellent qualitative agreement between our model and the experimental data. In the limit of $f\rightarrow 0$, Eq. (18) predicts the plateau value of the real part to be given by

$$\mathrm{Re}\{\chi_{nc}(f\rightarrow 0)\}=\frac{\alpha C_{ox}C_{cox}}{\alpha C_{ox}+\beta C_{cox}}. \tag{22}$$

Equation (18) also yields a peak in the imaginary part, whose position can be calculated by simple functional analysis to

$$2\pi f_p=-g\frac{\alpha C_{ox}+\beta C_{cox}}{q\alpha\beta C_{cox}}. \tag{23}$$

Using the value of β obtained from standard MOS equations for the experimental value of V_{FB0}, Eqs. (22) and (23) can be used to extract the parameters α and g from the measured spectra. The experimental data of V_{FB0}, $\mathrm{Re}\{\chi_{nc}(f\rightarrow 0)\}/C_{cox}$, and f_p, as well as the extracted parameters α, β, and g are listed in Table II for sample nNC1 and in Table III for samples nNC2 and nNC3. However, there are some differences between the theoretical and measured behavior of $\chi_{nc}(f)$ [Fig. 6(c)]. The observed peak in the imaginary part is lower and broader than the calculated one. We remark that Eq. (18) predicts $\mathrm{Im}\{\chi_{nc}(f_p)\}=-1/2\ \mathrm{Re}\{\chi_{nc}(f\rightarrow 0)\}$. The measured spectrum of the real part seems to be contorted as compared to the theoretical prediction. These differences are reminiscent of the findings of impedance measurements on standard MOS capacitors.[43] In these systems, it is well known that lateral fluctuations of the surface potential φ_s causes a broadening of the peak in the impedance spectra. For our samples, lateral fluctuations of φ_s mainly arise from

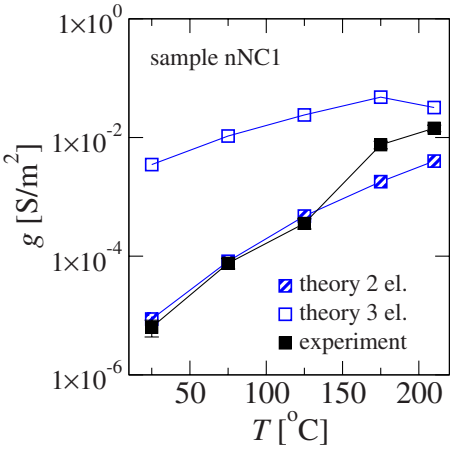

FIG. 7. (Color online) Comparison of the experimental and theoretical values of the small-signal conductance g for different temperatures (sample nNC1 and $V_{GB0}=1$ V). The experimental values of g were extracted from the values of f_p according to Eq. (23). The calculations were performed under the assumption of $N=2$ and $N=3$ electrons stored per nanocrystal.

the spatially inhomogeneous charge distribution in the gate oxide since the electrons are localized in the nanocrystals. We have verified this effect in a previous work.[34] In terms of the model presented here, the fluctuations of φ_s^0 implies a fluctuation in β. Indeed, if one takes them into account by assuming a Gaussian distribution of φ_s^0, our model describes also quantitatively the experimental data for a standard deviation $\sigma_{\varphi_s}=0.14\times\bar{\varphi}_s^0$ [dashed line in Fig. 6(c)]. The lateral distribution of the inversion charge in the substrate adapts to the lateral distribution of the surface potential and thus compensates the fluctuation in φ_s^0 to a certain extent. With increasing temperature, the electron density in the channel increases, yielding a more effective compensation of the fluctuation in φ_s^0. This explains why the shape of the spectra of $\chi_{nc}(f)$ becomes more similar to the theoretical behavior for increasing temperature [Fig. 6(a)]. However, lateral fluctuations of φ_s^0 cannot explain why the shape of the spectra of $\chi_{nc}(f)$ changes with increasing tunnel oxide thickness [Fig. 6(b)]. This may be caused by an additional effect. Probably, the size distribution of the NCs implies a certain distribution in the tunnel distances, which has a stronger effect for larger values of $\langle d_{tox}\rangle$.[42]

Figure 7 compares the values of the small-signal conductance g extracted from the experiments with the respective values calculated from Eq. (8). The theoretical values are very sensitive to the number of electrons per NC assumed in the calculations. There is an excellent agreement for $N=2$ electrons per NC. For $N=3$, the agreement is partial. From our measured V_{FB0} values (Fig. 5), however, one obtains approximately three rather than two electrons per nanocrystal within the framework of the charge-sheet approximation [Eq. (1)]. We attribute the difference between the experimental and the theoretical value of g mainly to the limited accuracy of the determination of the number of electrons per NC implicit in the charge-sheet approximation. Furthermore, the accuracy of the quantum-mechanical calculation is also limited due to the constraints of the model [assumption (iv)].

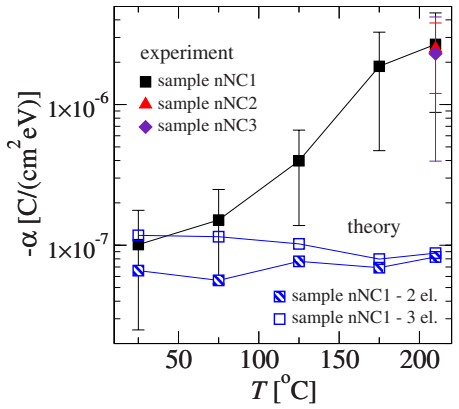

FIG. 8. (Color online) Comparison of the experimental value of α_{total} and the values of $\alpha_{\text{nc}}^{\text{ideal}}$ calculated by DFT. The theoretical data refer to sample nNC1 with different numbers of electrons ($N=2$ and $N=3$) assumed per NC. α_{total} was extracted from the value of $\text{Re}\{\chi_{\text{nc}}(f\rightarrow 0)\}/C_{\text{cox}}$ using Eq. (22).

However, the agreement between the theoretical and experimental values of g, in particular the prediction of the correct temperature dependence of g by the model, verifies the validity of the underlaying assumptions. The charging and discharging processes are, indeed, dominated by the transitions between the quantized cluster states and the Si conduction band, while direct transitions between the Ge-NC/SiO_2 interface states and the Si conduction band play a minor role. The almost exponential temperature dependence of g can be attributed to the term in Eq. (8) originating from the first derivative of the Fermi distribution, while the coupling matrix elements $M_{m,n}$, the energy eigenvalues $E_{m(n)}$ and the eigenstates $\psi_{m(n)}$ only weakly depend on temperature.

Figure 8 compares the values of α_{total} extracted from the experimental data with the contribution $\alpha_{\text{nc}}^{\text{ideal}}$ of the quantized cluster states calculated according to Eq. (21). The values of $\alpha_{\text{nc}}^{\text{ideal}}$ for two and three electrons stored in the nanocrystal do not differ strongly from each other. For 25 °C, the theoretical values of $\alpha_{\text{nc}}^{\text{ideal}}$ agree fairly well with the values α_{total} extracted from the experiment. However, $\alpha_{\text{nc}}^{\text{ideal}}$ and α_{total} exhibit a totally different temperature behavior. While α_{total} strongly increases with increasing T, $\alpha_{\text{nc}}^{\text{ideal}}$ decreases. For 210 °C, $\alpha_{\text{nc}}^{\text{ideal}}$ is two orders of magnitude smaller than α_{total}. The same result was obtained for sample nNC2 and sample nNC3 (Table III). We interpret this observation as follows: At room temperature, assumption (iii) does not seem to be valid. The time scales of capture (emission) of electrons by the traps from (to) the quantized states in the conduction band of the NC seem to be comparable to or larger than the time scales of tunneling from (to) the cluster states to (from) the inversion channel. Therefore, the alternating external field modulates only the charge stored in the quantized cluster states but does not modulate the charge stored in the Ge-NC/SiO_2 interface traps. In this case, α_{total} corresponds to $\alpha_{\text{nc}}^{\text{ideal}}$. For increasing temperature, the position of the extrapolated quasi-Fermi level of the substrate within the band gap of the NC shifts toward lower energies. Since $\alpha_{\text{nc}}^{\text{ideal}}$ strongly depends on $E_{Fn}^{\text{nc},0}$, its value decreases with increasing temperature. In the real system, this effect is obviously overcompensated by the increasing contribution of the Ge-NC/SiO_2 interface states due to decreasing time scales of capture (emission) by (from) these traps. Thus, α_{total} increases with increasing T. This interpretation is consistent with relatively long electron emission times $>10^3$ s from the traps, which had been observed in the large signal discharging characteristic of our samples.[44] However, there is an apparent contradiction to the estimation $<10^{-3}$ s of the upper limit of electron capture times based on the results of the photoluminescence measurements (Sec. II C). We tentatively explain this discrepancy with the energy distribution of the Ge-NC/SiO_2 interface states within the band gap of the NC. The shallow traps energetically located close to the lowest quantized state in the conduction band of the NC may exhibit very short electron capture times smaller than the radiative lifetimes. In our small-signal measurements, the electrons can be expected to thermalize from these shallow traps to interface states energetically located in the vicinity of $E_{Fn}^{\text{nc},0}$. From these deep trap states, the electron emission rate is very small at room temperature.

In order to estimate the projected density N_{it} of the Ge-NC/SiO_2 interface states, we focus on the α values obtained for 210 °C since α_{total} (210 °C) is expected to include the maximum contribution of the traps. From Eq. (14) one obtains $\tilde{N}_{\text{it}}=1.7\times 10^{13}$ $\text{cm}^{-2}\,\text{eV}^{-1}$ in the vicinity of $E_{Fn}^{\text{nc},0}$. Note that due to the charge-sheet approximation this value for $\tilde{N}_{\text{it}}$ corresponds to a projection of all states into a plane within the gate oxide, parallel to the Si substrate. Assuming the traps to be exclusively located at the Ge-NC/SiO_2 interface (neglect of traps in the volume of the NCs), one can recalculate the real Ge-NC/SiO_2 interface state density to be $N_{\text{it}}=2.8\times 10^{13}$ $\text{cm}^{-2}\,\text{eV}^{-1}$. This high value of the interface trap density is consistent with the absence of any photoluminescence attributable to band-to-band transition in the Ge-NCs (Sec. II C). This observation furthermore agrees with the results of structural investigations of the Ge-NC/SiO_2 interface,[28] and with various phenomena observed in the transient charging and discharging characteristics of the Ge-NCs.[34,44] Again, one should note that this high Ge-NC/SiO_2 interface state density is obtained for samples which experienced a hydrogen passivation at 450 °C prior the measurements. Obviously, this yields no or only an incomplete hydrogen passivation of the Ge-NC/SiO_2 matrix interface states. This observation is reminiscent of the findings of Kan *et al.*,[45] who found that a forming gas anneal at 450 °C did not affect the $C(V)$ behavior of MOS capacitors containing Ge NCs embedded in the gate oxide.

V. CONCLUSIONS

We have investigated quantitatively the electronic properties of the interface between Ge nanocrystals and a SiO_2 matrix by analyzing the frequency-dependent response of charge stored in the NCs to an alternating external field. The small-signal response of the cluster charge can be understood within the framework of a relatively simple model obtained from a first-order expansion of a general quantum-mechanical description of the system. The most important model parameter, the derivative of the cluster charge with respect to the position of the quasi-Fermi level in the nano-

crystal, was extracted from the experiments and calculated by density-functional theory. Since the model calculation considers only charge storage in the quantized NC states and disregards trap states at the Ge-NC/SiO_2 interface, the contribution of the traps shows up in the difference of both values. We obtained a high Ge-NC/SiO_2 interface state density of 2.8×10^{13} cm^{-2} eV^{-1}. This finding is consistent with the absence of any photoluminescence attributable to the NCs, possibly a consequence of efficient trap-mediated nonradiative recombination processes. The high density of states at the Ge-NC/SiO_2 interface poses a serious problem for the application of the Ge-NC:SiO_2 system in optoelectronics and in photovoltaics. Due to the efficient non-radiative processes mediated by these traps, the electroluminescence from the Ge NCs, as well the photocurrent extractable from the Ge NCs can be expected to be only marginal. We hope that our work provides stimulus for further investigations into the physical nature of the Ge-NC/SiO_2 interface states, e.g., by atomistic theoretical investigations or by electron spin-resonance measurements. This knowledge could show a way how these interface states can be passivated. Alternatively, the Ge-NC/matrix interface properties for an alternative matrix material, e.g., silicon nitride, could be also investigated. The measurement method presented in this work might be useful for these experiments.

ACKNOWLEDGMENTS

We thank E. Bugiel for the TEM investigations, and R. Rölver for the PL measurements. This work was funded by Deutsche Forschungsgemeinschaft under Grant No. HO 1885/8-3. J.S.d.S. is indebted to the Brazilian National Research Council (CNPq) for financial support.

*peibst@mbe.uni-hannover.de

[1] H. I. Hanafi, S. Tiwari, and I. Khan, IEEE Trans. Electron Devices **43**, 1553 (1996).
[2] Y.-C. King, T.-J. King, and C. Hu, IEEE Trans. Electron Devices **48**, 696 (2001).
[3] M. Kanoun, C. Busseret, A. Poncet, A. Souifi, T. Baron, and E. Gautier, Solid-State Electron. **50**, 1310 (2006).
[4] Y. Maeda, Phys. Rev. B **51**, 1658 (1995).
[5] S. Takeoka, M. Fujii, S. Hayashi, and K. Yamamoto, Phys. Rev. B **58**, 7921 (1998).
[6] M. Scarselli, S. Masala, P. Castrucci, M. De Crescenzi, E. Gatto, M. Venanzi, A. Karmous, P. D. Szkutnik, A. Ronda, and I. Berbezier, Appl. Phys. Lett. **91**, 141117 (2007).
[7] B. Sun, G. Zou, X. Shen, and X. Zhang, Appl. Phys. Lett. **94**, 233504 (2009).
[8] D. Riabinina, C. Durand, M. Chaker, N. Rowell, and F. Rosei, Nanotechnology **17**, 2152 (2006).
[9] J. H. Chen, Y. Q. Wang, W. J. Yoo, Y.-C. Yeo, G. Samudra, D. S. H. Chan, A. Y. Du, and D.-L. Kwong, IEEE Trans. Electron Devices **51**, 1840 (2004).
[10] Y. M. Niquet, G. Allan, C. Delerue, and M. Lannoo, Appl. Phys. Lett. **77**, 1182 (2000).
[11] A. Konchenko, Y. Nakayama, I. Matsuda, S. Hasegawa, Y. Nakamura, and M. Ichikawa, Phys. Rev. B **73**, 113311 (2006).
[12] S. Takeoka, M. Fujii, S. Hayashi, and K. Yamamoto, Appl. Phys. Lett. **74**, 1558 (1999).
[13] K. Seino, F. Bechstedt, and P. Kroll, Nanotechnology **20**, 135702 (2009).
[14] M. Luppi and S. Ossicini, Phys. Rev. B **71**, 035340 (2005).
[15] R. Soulairol and F. Cleri, Solid State Sci. **12**, 163 (2010).
[16] F. Djurabekova and K. Nordlund, Phys. Rev. B **77**, 115325 (2008).
[17] G. Hadjisavvas and P. C. Kelires, Phys. Rev. Lett. **93**, 226104 (2004).
[18] H. Takagi, H. Ogawa, Y. Yamazaki, A. Ishizaki, and T. Nakagiri, Appl. Phys. Lett. **56**, 2379 (1990).
[19] L. Pavesi, L. Dal Negro, C. Mazzoleni, G. Franzo, and F. Priolo, Nature (London) **408**, 440 (2000).
[20] R. J. Walters, G. I. Bourianoff, and H. A. Atwater, Nature Mater. **4**, 143 (2005).
[21] M. H. Liao, C.-Y. Yu, T.-H. Guo, C.-H. Lin, and C. W. Liu, IEEE Trans. Electron Devices **27**, 252 (2006).
[22] K. S. Min, K. V. Shcheglov, C. M. Yang, H. A. Atwater, M. L. Brongersma, and A. Polman, Appl. Phys. Lett. **68**, 2511 (1996).
[23] J. G. Couillard and H. G. Craighead, J. Mater. Sci. **33**, 5665 (1998).
[24] N. L. Rowell, D. J. Lockwood, A. Karmous, P. D. Szkutnik, I. Berbezier, and A. Ronda, Superlattices Microstruct. **44**, 305 (2008).
[25] E. L. de Oliveira, E. L. Albuquerque, J. S. de Sousa, and G. A. Farias, J. Appl. Phys. **103**, 103716 (2008).
[26] B. H. Koh, E. W. H. Kan, W. K. Chim, W. K. Choi, D. A. Antoniadis, and E. A. Fitzgerald, J. Appl. Phys. **97**, 124305 (2005).
[27] Y. Shi, K. Saito, H. Ishikuro, and T. Hiramoto, J. Appl. Phys. **84**, 2358 (1998).
[28] R. Peibst, T. Dürkop, E. Bugiel, A. Fissel, I. Costina, and K. R. Hofmann, Phys. Rev. B **79**, 195316 (2009).
[29] N. Daldosso, M. Luppi, S. Ossicini, E. Degoli, R. Magri, G. Dalba, P. Fornasini, R. Grisenti, F. Rocca, L. Pavesi, S. Boninelli, F. Priolo, C. Spinella, and F. Iacona, Phys. Rev. B **68**, 085327 (2003).
[30] M. Schmidt, L. Korte, A. Laades, R. Stangl, C. Schubert, H. Angermann, E. Conrad, and K. Maydell, Thin Solid Films **515**, 7475 (2007).
[31] L. Korte and M. Schmidt, J. Non-Cryst. Solids **354**, 2138 (2008).
[32] T. Dürkop, E. Bugiel, I. Costina, A. Ott, R. Peibst, and K. R. Hofmann, Mater. Sci. Eng., B **147**, 213 (2008).
[33] Y. Liu, S. Tang, and S. K. Banerjee, Appl. Phys. Lett. **88**, 213504 (2006).
[34] R. Peibst, M. Erenburg, E. Bugiel, and K. R. Hofmann, J. Appl. Phys. **108**, 054316 (2010).
[35] S. Tiwari, F. Rana, H. I. Hanafi, E. F. Crabbe, and K. Chan, Appl. Phys. Lett. **68**, 1377 (1996).
[36] J. S. de Sousa, A. V. Thean, J. P. Leburton, and V. N. Freire, J.

Appl. Phys. **92**, 6182 (2002).
[37] J. S. de Sousa, V. N. Freire, and J. P. Leburton, Appl. Phys. Lett. **90**, 223504 (2007).
[38] J. S. de Sousa, V. N. Freire, and E. F. da Silva, Jr., Appl. Surf. Sci. **234**, 218 (2004).
[39] C. Cai and C. T. Sah, J. Appl. Phys. **89**, 2272 (2001).
[40] W. A. Harrison, Phys. Rev. **123**, 85 (1961).
[41] S. Tiwari, F. Rana, K. Chan, L. Shi, and H. I. Hanafi, Appl. Phys. Lett. **69**, 1232 (1996).
[42] V. Beyer, J. V. Borany, and M. Klimenkov, J. Appl. Phys. **101**, 094507 (2007).
[43] B. H. Nicollian and A. Goetzberger, Bell Syst. Tech. J. **XLVI**, 1055 (1967).
[44] J. S. de Sousa, R. Peibst, M. Erenburg, E. Bugiel, G. A. Farias, J. P. Leburton, and K. R. Hofmann, IEEE Trans. Electron Devices (to be published).
[45] E. W. H. Kan, W. K. Choi, W. K. Chim, E. A. Fitzgerald, and D. A. Antoniadis, J. Appl. Phys. **95**, 3148 (2004).